

Synoptic-scale precursors of landslides in the western Himalaya and Karakoram

Article

Accepted Version

Creative Commons: Attribution-Noncommercial-No Derivative Works 4.0

Hunt, K. ORCID: <https://orcid.org/0000-0003-1480-3755> and Dimri, A. P. (2021) Synoptic-scale precursors of landslides in the western Himalaya and Karakoram. *Science of the Total Environment*, 776. 145895. ISSN 0048-9697 doi: 10.1016/j.scitotenv.2021.145895 Available at <https://centaur.reading.ac.uk/96224/>

It is advisable to refer to the publisher's version if you intend to cite from the work. See [Guidance on citing](#).

To link to this article DOI: <http://dx.doi.org/10.1016/j.scitotenv.2021.145895>

Publisher: Elsevier

All outputs in CentAUR are protected by Intellectual Property Rights law, including copyright law. Copyright and IPR is retained by the creators or other copyright holders. Terms and conditions for use of this material are defined in the [End User Agreement](#).

www.reading.ac.uk/centaur

Central Archive at the University of Reading

Reading's research outputs online

Synoptic-scale precursors of landslides in the western Himalaya and Karakoram

Kieran M. R. Hunt¹ and A. P. Dimri²

¹*Department of Meteorology, University of Reading, UK*

²*School of Environmental Sciences, Jawaharlal Nehru University, Delhi, India*

Abstract

In the Upper Indus Basin (UIB), precipitation associated with synoptic-scale circulations impinges on the complex and steep orography of the western Himalaya and Karakoram. Heavy rainfall often falls over the foothills, frequently triggering landslides there. This study explores the role of these synoptic-scale circulations – extratropical western disturbances (WDs) and tropical depressions (TDs) – in producing the conducive conditions necessary to trigger landslides, using data from the NASA Global Landslide Catalog and WD and TD track databases.

During the winter (October to April), UIB landslides peak in February and occur at a rate of 0.05 day^{-1} , 61% of which are associated with the passage of a WD. They are most common when a WD is located within a few hundred kilometres of 30°N , and significantly rarer if the WD is north of 40°N . WDs provide moist southwesterly flow from the Arabian Sea (AS) and Mediterranean Sea to the UIB, resulting in large-scale precipitation, but landslide probability is not related to WD intensity. Non-WD winter landslides are associated with small-scale orographic precipitation that we hypothesise is due to cloudbursts.

During the summer (May to September), UIB landslides peak in August and occur at a rate of 0.11 day^{-1} , 60% of which are associated with TD activity. Many of these TDs are found over central India, slightly south of the climatological monsoon trough, where they provide strong monsoonal southeasterlies to the UIB flowing along the Himalayas. Increased landslide frequency is also associated with TD activity over the southern Bay of Bengal (BoB), and it is hypothesised that this is related to monsoon break conditions. Landslide frequency is significantly correlated with TD intensity. Non-TD landslides are associated with a northwestward extension of the monsoon trough, providing southeasterly barrier flow to the UIB.

Implications for forecasting and climate change are discussed.

Keywords: landslides; Indus Basin; western disturbances; depressions; precipitation; moisture flux

1 Introduction

2 About 75% of all global landslides occur in Asia; of
3 these, the majority happen along the mountain ranges
4 of south Asia: the Himalaya, the Hindu Kush, and the
5 Karakoram (Froude and Petley, 2018). Along most
6 of the Himalaya, the seasonality of landslides is de-
7 termined by the arrival and withdrawal of the sum-
8 mer monsoon (Kirschbaum et al., 2010; Petley, 2012).
9 However, further west, over the western Himalaya and
10 Karakoram, the influence of the monsoon is less impor-
11 tant, and landslides become increasingly frequent in the
12 winter and spring months (Atta-ur Rehman et al., 2011;
13 Saleem et al., 2020). This results in a complex seasonal-
14 ity of landslides in the Upper Indus Basin (UIB) (Fig. 1)
15 which makes adequate preparation and mitigation a
16 challenge. Over the UIB, landslides have been responsi-
17 ble for changing the course of Indus tributaries (Hewitt,
18 1998), significant loss of life (Kirschbaum et al., 2012;
19 Froude and Petley, 2018) and significant socioeconomic
20 damage (Atta-ur Rehman et al., 2011).

21 Weather patterns over the Indus Basin are highly sea-
22 sonal. In the winter (October to April, i.e. outside of
23 the monsoon season), mean low-level winds are weakly
24 westerly with a strong upper-level westerly jet. Within
25 this jet, extratropical cyclones, known as western dis-
26 turbances (WDs), are embedded, and are responsible
27 for most winter precipitation in this region. In summer
28 (May to September), the westerly jet migrates poleward
29 and the frequency of WDs reduces dramatically. In-
30 stead, precipitation usually occurs as a result of north-
31 westward extensions of monsoon activity. Tropical de-
32 pressions (TDs) are responsible for about half of sum-
33 mer monsoon precipitation, though the fraction is gen-
34 erally slightly lower over the Indus Basin (Hunt and
35 Fletcher, 2019). Climatological precipitation, which is
36 greatest along the foothills, is shown for both winter

37 and summer in the middle panels of Fig. 2. Many pre-
38 vious studies agree that heavy rainfall is the most im-
39 portant environmental precursor to landslides globally
40 (Kirschbaum et al., 2012, 2015), especially over south
41 Asia (Dahal et al., 2008; Kirschbaum et al., 2010; Zhang
42 et al., 2019), where intensity–duration thresholds are
43 usually used as predictors with some success (Sengupta
44 et al., 2010; Kirschbaum et al., 2011). It is also impor-
45 tant that there has been significant antecedent rainfall
46 so that the soil is either nearly or totally saturated (Ga-
47 bet et al., 2004; Ahmed et al., 2014; Kumar et al., 2014),
48 although the relative importance is highly sensitive to
49 surficial geology. A few case studies of particularly sig-
50 nificant flooding and landslide events across the west-
51 ern Himalaya have looked for meteorological precursors.
52 For example, the heavy rainfall that caused extensive
53 flash flooding and landslides over Jammu and Kashmir
54 in 2010 were ascribed to multiple mesoscale convective
55 storms that were steered into the region by favourable
56 mid-tropospheric jet. These coincided with southerlies
57 from the Arabian Sea (AS), which provided the mois-
58 ture required for unusually sustained, heavy rainfall
59 (Kumar et al., 2014). Analysis of the 2013 Uttarak-
60 hand floods and associated landslides found the an-
61 tecedent rainfall came about as a strong WD interacted
62 with a TD, providing very large southeasterly moisture
63 flux to the orography (Mishra, 2015; Chevuturi and
64 Dimri, 2016; Hunt et al., 2020a). More generally, moist
65 southwesterlies embedded in WDs (Dimri et al., 2015)
66 provide heavy rainfall and sometimes cloudbursts due
67 to conjugate factors of convective triggering and oro-
68 graphic locking (Dimri et al., 2017).

69 Heavy rainfall is not the only important ingredient
70 for landslides. As mentioned earlier, the soil and un-
71 derlying rock must usually be very close to field ca-
72 pacity before the shear strength within a slope is re-
73 duced enough for landslides to be initiated. In some

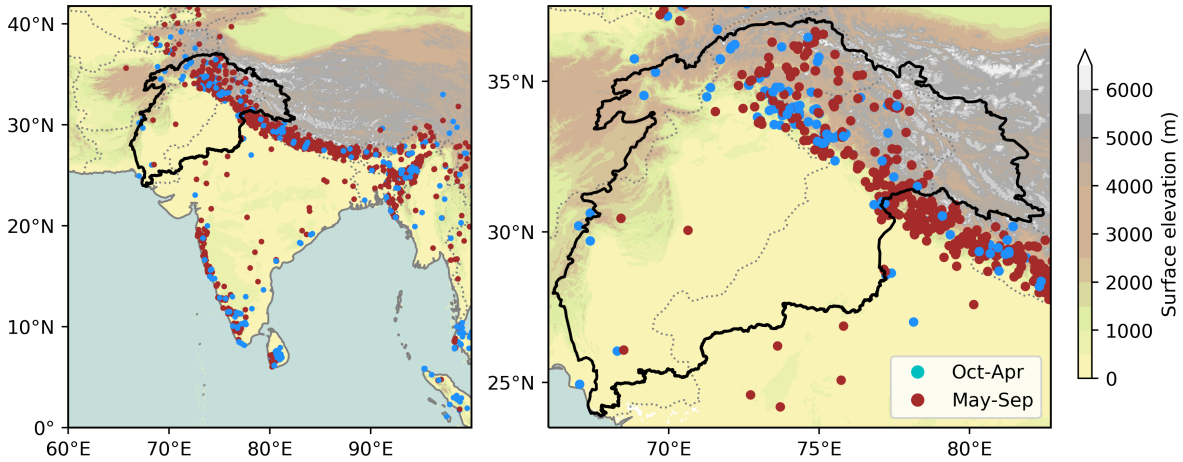


Figure 1: Locations of landslides in the NASA GLC, covering 2007-2015. Blue dots mark landslides occurring between October and April; brown dots mark those occurring between May and September. The thick black line marks the boundary of the Indus Basin. Left: over the Indian peninsula and surrounding area; right: over the Indus Basin (marked in black).

locations may only be possible near the end of the wet season. For example, Gabet et al. (2004) found that a mean seasonal rainfall of 860 mm was required to get the regolith up to field capacity over Nepal and as a result, landslides peak there during the latter part of the summer monsoon. Even then, several environmental and geological factors must be taken into consideration. A review of global landslide research by Zhang et al. (2019) noted that slope gradient and underlying lithology were important in determining landslide size, whereas climatological rainfall was important in determining their location. Looking specifically at the UIB, a detailed study by Ahmed et al. (2014) explored factors controlling landslide susceptibility. They separated their analysis into environmental and causative risk factors. For environmental factors, they found that UIB landslides were most common on slopes with an angle between 30° and 45° , at elevations between 2 and 4 km. They also found a significant, though less important, relationship with slope aspect, finding that landslides were most common on slopes facing a heading of 226° – 270° – this is the orientation at which moist southwestlies, often induced by passing WDs, would strike the orography head on. Ghosh et al. (2011) found similar results for the eastern Himalaya near Darjeeling, also

highlighting the role of lithology, geomorphology, and land use. These environmental factors are useful in understanding the spatial patterns of landslide frequency, and thus are important in reducing false alarms. However, being quasi-static, they are not useful for predicting when landslides might occur. Causative risk factors, on the other hand, provide temporal information and are thus potentially useful for predictions through an understanding of the underlying meteorology.

Despite the global and regional linkages with heavy rainfall and the case studies discussed earlier, very little work has been done to assess meteorological precursors to landslides in south Asia over climatological sample sizes. Kamae et al. (2017) found that atmospheric rivers were important in providing the heavy precipitation needed to trigger landslides over East Asia. Mamadjanova et al. (2018) found that moist westerlies were an important precursor for landslides in Uzbekistan and assessed the relative role of cyclonic circulations. Saleem et al. (2020) noted that WDs play an “equal role” to monsoonal rainfall in instigating landslides over northern Pakistan.

A full understanding of the meteorological precursors of landslides is a vital component in constraining their sensitivity to climate change, in particular be-

cause synoptic-scale systems contribute a majority of average precipitation and extreme precipitation events to the Himalaya (Hunt et al., 2018b, 2019b; Hunt and Fletcher, 2019). For example, monsoon depressions are projected to fall in frequency, but move poleward (Sandee et al., 2018); and WDs are projected to bring more intense rainfall (Hunt et al., 2020b), though the fate of their frequency in a changing climate remains an open question (Ridley et al., 2013; Krishnan et al., 2018; Hunt et al., 2019a). Correspondingly, Kirschbaum et al. (2020) found a projected increase in landslides over the Himalaya when they applied a landslide hazard model to global climate model output. Increases in the observational record have been found for the central Himalaya (Petley et al., 2007) and the Hindu-Kush Himalaya (You et al., 2017); though Petley et al. (2007) attributed the increase in their record to be due to increased construction and infrastructure work on slopes.

The key research questions to be addressed, therefore, are:

- What role does the presence of synoptic-scale systems, such as TDs and WDs, play in initiating landslides over the western Himalaya and Karakoram, in particular over the UIB?
- Are there other weather patterns that act as important precursors?
- Can this information be used to improve landslide predictability?

2 Data and methodology

2.1 NASA Global Landslide Catalogue

In this study, we use landslide data from the NASA Global Landslide Catalogue (GLC, Kirschbaum et al., 2010, 2015). The GLC is a catalogue of precipitation-triggered landslides identified from sources including

news reports, disaster databases, and research papers. Triggers are determined from the source material itself. The catalogue contains over 11000 entries from 2007 to 2015, 327 of which occur in the UIB. Uncertainty in recorded location is also included within the GLC. Of the 327 UIB landslides, 88% have a location uncertainty of less than 50 km, 70% within 25 km, and 45% within 10 km. 11% lack spatial uncertainty data. Each landslide is assigned a UTC day-of-occurrence, but uncertainty in temporal information is not provided. We do not expect spatiotemporal uncertainties to significantly affect our results. However, it is worth noting here that the nature of the sources used in the GLC impart a bias towards populated regions – where landslides are more likely to be reported – and hence towards more anthropogenic triggers. The GLC also includes a measure of ‘size’ for each landslide, ranging from small (shallow; affecting one hillslope; minimal or no infrastructure damage) to very large (multiple events affecting an entire region; catastrophic damage to infrastructure; often encompassing whole villages). Of the 327 UIB landslides in the catalogue, 14 are rated small, 284 medium, 26 large, and 3 very large. For more information on uncertainty and size measures, the reader is encouraged to read Secs. 2.1 and 2.2 of Kirschbaum et al. (2015).

2.2 ERA-Interim

To analyse the structure of dynamical fields and moisture in the atmosphere, we use the European Centre for Medium-Range Weather Forecasts Interim reanalysis (ERA-I; Dee et al., 2011). All fields are available at six-hourly intervals with a horizontal resolution of T255 (~ 78 km at the equator), with the three-dimensional fields further distributed over 37 vertical levels spanning from the surface to 1 hPa. Data are assimilated into the forecasting system from a variety of sources,

194 including satellites, ships, buoys, radiosondes, aircraft,
195 and scatterometers. In this study, we use wind and hu-
196 midity data at all pressure levels to compute vertically-
197 integrated moisture flux.

2.4 Track databases

We use the database of WD tracks from Hunt et al.
228 (2018a) in this study. Using six-hourly ERA-Interim
229 data, they tracked WDs by computing the mean relative
230 vorticity in the 450–300 hPa layer, then performed a
231 spectral truncation at T63 to filter out short-wavelength
232 noise. They then identified positive-definite vorticity
233 regions within this field and determined the centroid
234 location for each one. These centroids were then linked
235 in time, subject to constraints in distance and steering
236 winds, to form candidate WD tracks. Finally, those
237 candidate tracks that did not pass through South Asia
238 [20°N–36.5°N, 60°E–80°E], have a lysis to the east of
239 their genesis, or last at least 48 hours were rejected.
240 This catalogue is publicly available at <http://dx.doi.org/10.5285/233cf64c54e946e0bb691a07970ec245>.

We use the database of TD tracks from Hunt
243 and Fletcher (2019) in this study. The core of the
244 algorithm used for this is identical to that used to
245 develop the WD catalogue above, except the input
246 is the truncated 900–800 hPa relative vorticity field.
247 There is no domain filtering at the end but tracks
248 shorter than 48 hours are still rejected. This catalogue
249 is publicly available at http://gws-access.jasmin.ac.uk/public/incompass/kieran/track_data/lps-tracks_v1_1979-2014.csv. Note that in this study,
250 *tropical depression* is used as a collective term to
251 refer to monsoon low-pressure systems, monsoon
252 depressions, tropical lows, and tropical storms.

3 Results

As discussed in the introduction, the overwhelming ma-
257 jority of landslides in the Himalaya occur after heavy
258 precipitation. To show what form it takes, mean pre-
259 cipitation is plotted for days on which a landslide oc-
260 curs in the Upper Indus Basin (UIB; an area that con-
261

198 2.3 GPM-IMERG

199 For our precipitation dataset, we use the gridded sur-
200 face product Integrated Multi-Satellite Retrievals for
201 GPM (IMERG; Huffman et al., 2015). This has global
202 coverage at a half-hourly, 0.1° resolution, starting June
203 2000 and continuing to the present day. Over the trop-
204 ics, IMERG primarily ingests retrievals from (for 2000–
205 2014) the now-defunct Tropical Rainfall Measuring Mis-
206 sion (TRMM; Kummerow et al., 1998, 2000) 13.8 GHz
207 precipitation radar and microwave imager (Kozu et al.,
208 2001) and (for 2014–) the Global Precipitation Mea-
209 surement (GPM; Hou et al., 2014) Ka/Ku-band dual-
210 frequency precipitation radar. Where an overpass is
211 not available, precipitation is estimated by calibrat-
212 ing infrared measurements from geostationary satel-
213 lites. While GPM-IMERG performs well when com-
214 pared against gauge-based products, performance falls
215 at higher elevations or when quantifying extreme rain-
216 fall events (anj; Prakash et al., 2018). Given the nature
217 of our study, this introduces some uncertainty into our
218 results. As such, all key results are additionally verified
219 using precipitation output from the Indian Monsoon
220 Data Assimilation and Analysis (IMDAA) reanalysis
221 project (Ashrit et al., 2020), as high resolution reanaly-
222 ses have been shown to perform well in the Indus Basin
223 (Baudouin et al., 2020). Full half-hourly resolution is
224 used in the antecedent rainfall analysis in Fig. 8, but
225 daily accumulations (00UTC–00UTC) are used for the
226 composite analysis in Figs. 2 and 6.

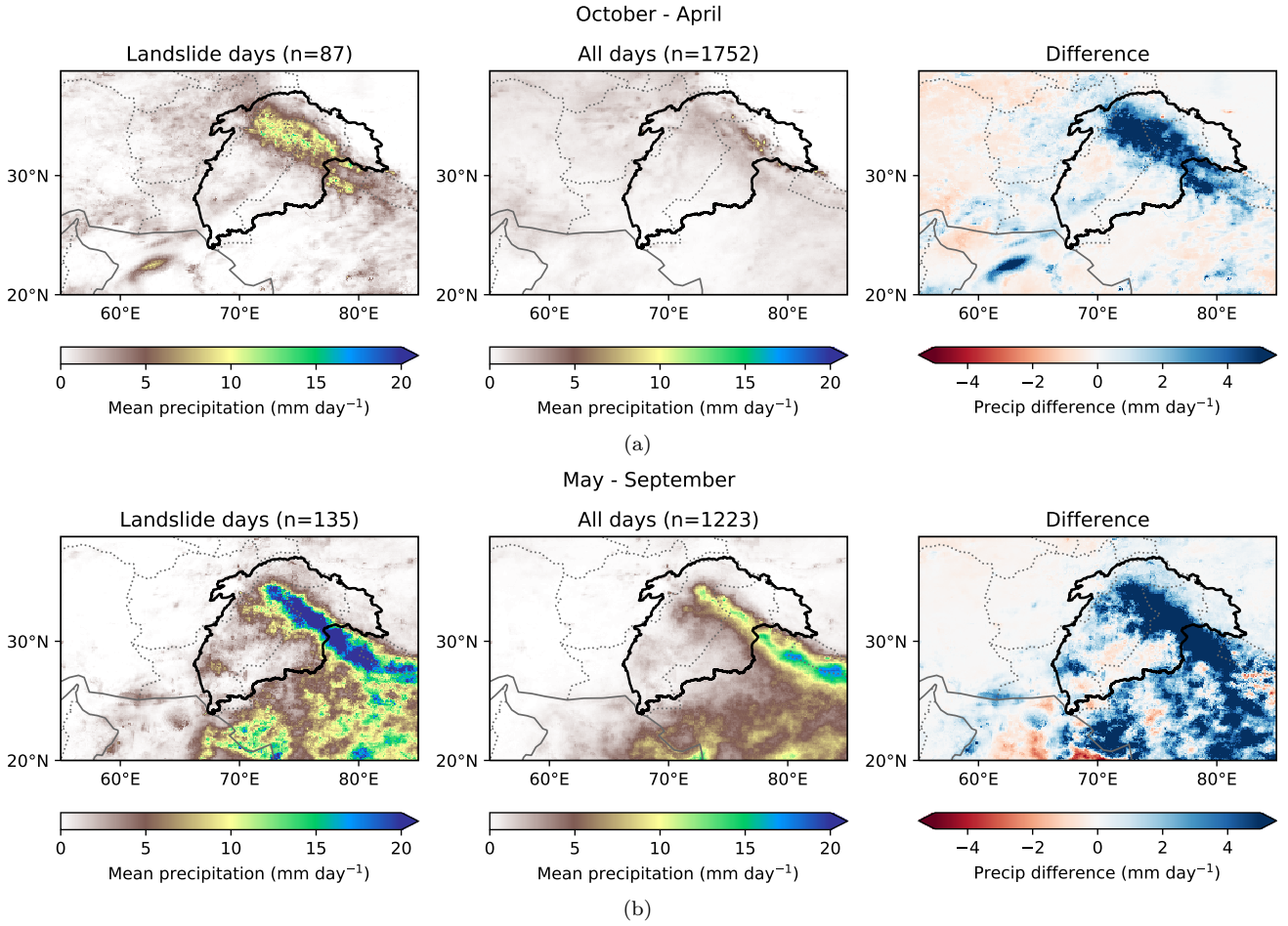


Figure 2: Mean precipitation for days in (a) October–April and (b) May–September in which a landslide occurs in the UIB (left panels) compared with the mean for all days in the same period (2007–2015, middle panels). Difference plots shown on the right. Data from GPM-IMERG. The solid black line marks the edge of the Indus River Basin. The same figure, computed using IMDAA reanalysis, is shown in supplementary Fig. S1.

tains both the western Himalaya and the Karakoram) in Fig. 2. For comparison, the precipitation climatology is shown, and the results are partitioned by season into the summer monsoon (May through September) and winter (October through April). Before proceeding, we remind the reader of the inherent uncertainties and biases present in the landslide dataset, as discussed in Sec. 2.1. Landslides are approximately twice as frequent in the UIB during the summer monsoon (occurring on 11% of days) as during the winter (occurring on 5% of days); this contrasts the central and eastern Himalaya, for which landslides almost exclusively occur during the summer monsoon (e.g. Kirschbaum et al., 2010). For a complete understanding of precursor weather, we must, therefore, consider the syn-

optic dynamics at work in both seasons. Computing the dispersion statistic, σ , (not shown), we find that UIB landslides are highly temporally clustered in the summer season ($\sigma \sim 4$), and quite temporally clustered in the winter season ($\sigma \sim 1.5$). It is evident from Fig. 2 that the precipitation is much heavier on landslide days in both seasons (in some places averaging 20 mm day⁻¹ more than the climatology). For events that occur during the summer monsoon (Fig. 2(b)), the anomalous precipitation has a footprint that extends southeast, far beyond the UIB, over the Indian subcontinent. This suggests that the anomalous rainfall over the UIB during the monsoon probably comes about as a result of enhanced monsoon activity, either through an active phase or through the passage of a monsoonal

292 tropical depression (TD). Disentangling active phases
293 of the monsoon from TD activity is difficult, and some
294 authors (e.g. Rajeevan et al., 2010) consider them to be
295 synonymous; however, TDs have been shown to provide
296 considerable monsoon rainfall to northwest India and
297 Pakistan if they sufficiently penetrate the subcontinent
298 or start in the Arabian Sea (Hunt and Fletcher, 2019).
299 It is reasonable, therefore, to assume that the source
300 of anomalous precipitation over the UIB during sum-
301 mer monsoon landslide is increased TD activity. For
302 winter landslides (Fig. 2(a)), the footprint of anom-
303 lous precipitation is, for the most part, confined to the
304 UIB, suggesting either a local source, or a more distant
305 source capable of providing significant moisture flux.
306 WDs are the predominant source of both climatolog-
307 ical precipitation and heavy precipitation events over
308 the winter UIB (e.g. Hunt et al., 2018b), but there are
309 other important sources such as non-WD cloudbursts
310 and orographic precipitation (Dimri, 2006).

311 3.1 Synoptic controls on landslide fre- 312 quency

313 We will now test the hypothesis that TDs and WDs
314 are responsible for the majority of monsoon and winter
315 landslides respectively in the UIB. Using the track cat-
316alogues described in Sec. 2.4, we find the nearest TD
317 or WD to each UIB landslide event. To identify the
318 nearest TD and WD, all track points for the respective
319 systems logged on the UTC day on which the landslide
320 occurred are considered. Among those, the point (one
321 for each type of system) with the shortest great-circle
322 distance to the landslide is used. The results that follow
323 in this study are not qualitatively sensitive to the choice
324 of temporal window. The distances between landslide
325 and system are tallied by month in Fig. 3. WDs have a
326 strong annual cycle and are most common in the win-
327 ter, and this projects strongly onto their relationship

328 with UIB landslide frequency (Fig. 3(a)). From Novem-
329 ber through May (narrowly excepting April), a WD is
330 present within 5000 km of a majority of UIB landslides.
331 Integrated over the non-monsoon months of October
332 to May, this value is 61%, of which 45% occur within
333 2000 km. TDs also have a strong annual cycle, al-
334 though they do continue in significant numbers outside
335 the monsoon. Again, this projects strongly onto their
336 relationship with UIB landslide frequency (Fig. 3(b)), a
337 TD is present with 5000 km of 60% of all UIB landslides
338 occurring between May and September, of which it is
339 within 2000 km 35% of the time. There is a secondary
340 peak of TD contribution in February and March, due
341 to pre-monsoon tropical cyclones in the Arabian Sea.

342 So, we have seen that landslide hazard in the UIB
343 has a relatively strong dependence on both the presence
344 and proximity of synoptic circulations such as WDs and
345 TDs. It is therefore reasonable to assume that land-
346 slides are also sensitive to system location. For ex-
347 ample, if a WD is too far east, then the associated
348 southerly moisture flux will impinge on the central or
349 eastern Himalaya instead of the western Himalaya, and
350 the chance of a landslide in the UIB will not be sig-
351 nificantly increased. To test this hypothesis, we use
352 the extract from the TD and WD track catalogues all
353 systems that occur during the GLC period (2007–2015).
354 Individual track points are then binned into $2^\circ \times 2^\circ$ grid-
355 boxes, and the mean frequency of UIB landslide occur-
356 rence given a system present in that gridbox is com-
357 puted. These maps, filtered by their respective seasons
358 (May–September for TDs; October–April for WDs) are
359 shown in Fig. 4. The map for WDs (Fig. 4(a)) has sev-
360 eral key features. Firstly, we see that the latitude of
361 the WD, tightly controlled by the latitude of the sub-
362 tropical westerly jet in which it is embedded (Dimri
363 and Chevuturi, 2016), is very important in determining
364 whether the likelihood of a UIB landslide is increased or

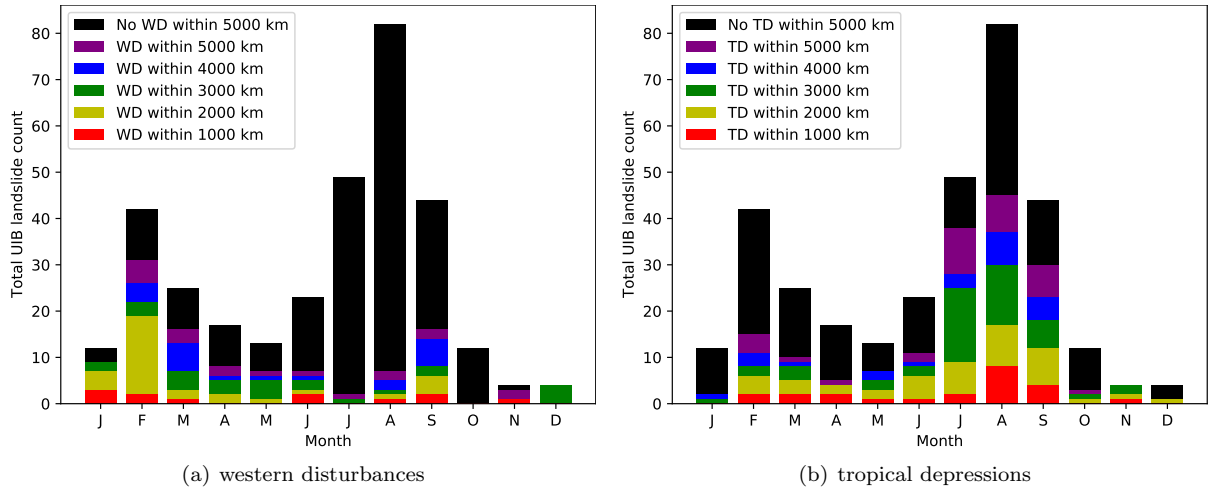


Figure 3: Monthly frequencies of landslides in the UIB. Bars coloured by proximity of (a) western disturbance and (b) tropical depression. Black indicates no system present within 5000 km of the landslide.

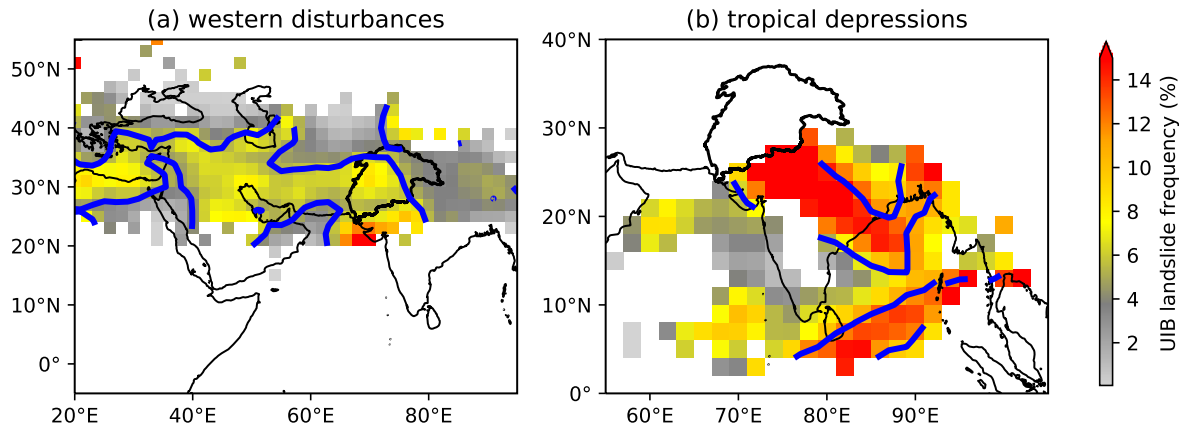


Figure 4: Mean likelihood of a landslide in the UIB, given presence of (a) a western disturbance in October–April or (b) a tropical depression in May–September in a given $2^\circ \times 2^\circ$ gridbox. The climatological values of $5\% \text{ day}^{-1}$ and $11\% \text{ day}^{-1}$ for October–April and May–September respectively are drawn with a solid blue line. Grid boxes with fewer than five systems in are not shown.

decreased. Systems within $3\text{--}4^\circ$ of 30°N result in a significantly increased chance of a UIB landslide, whereas those much further north, particularly beyond about 40°N , result in a significantly decreased chance. Secondly, there are three zonal maxima in frequency at about 30°E , 50°E , and 70°E respectively. This approximate wavelength of 2000 km corresponds to the spatial scale of WDs in the subtropical westerly jet (Rao and Srinivasan, 1969) and highlight the fact that when a WD is over, or very close to, the UIB, a younger one is often ~ 2000 km upstream. It is quite possible that these upstream WDs play an important role in triggering landslides over the UIB, and we will briefly discuss this in the next section; however a full treatment of the

role of coupled WD dynamics in bringing heavy precipitation to the Indus Basin is left for future work.

For monsoonal TDs (Fig. 4(b)), we see that proximity to the UIB is the most important parameter in increased landslide frequency. TDs aligned along the southern edge of the climatological monsoon trough result in UIB landslide frequencies of up to $20\% \text{ day}^{-1}$. Since TDs very rarely penetrate the subcontinent as far as the Indus Basin itself, they cannot provide the rain directly; instead, they must enhance the south-easterly monsoonal moisture flux that impinges on the UIB orography. This also explains why it is preferable for them to be near the south of the typical monsoon trough location; too far north and they would direct

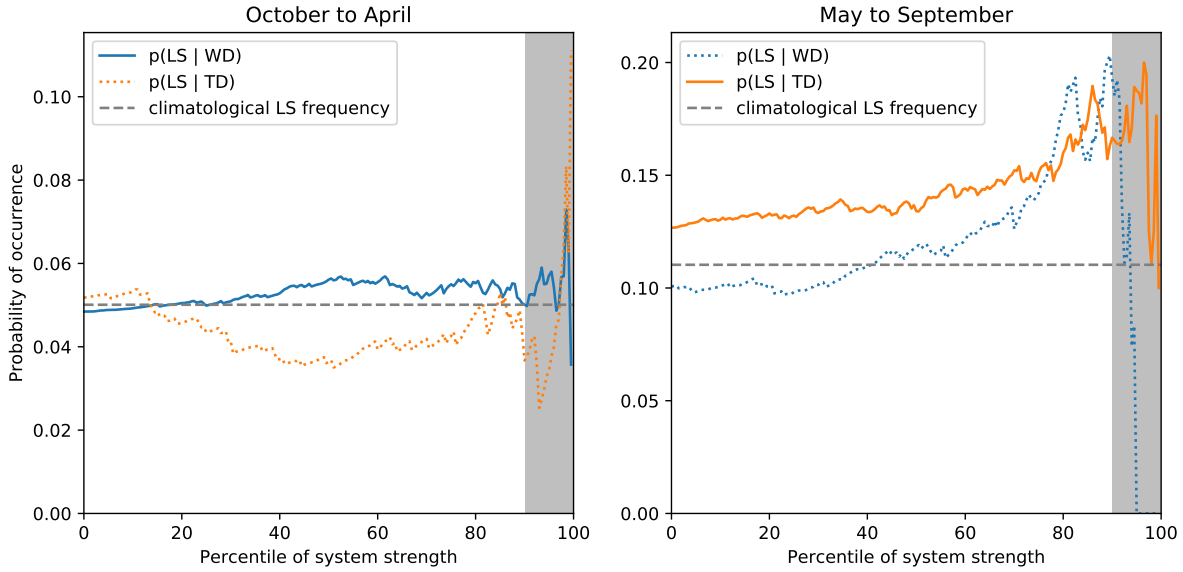


Figure 5: Change in likelihood of a landslide occurring in the UIB on a given day as a function of the intensity percentile of western disturbances (blue) and tropical depressions (orange) within 2000 km. For each season (October–April, left; May–September, right), the rarer type of system is plotted with a dotted line. A dashed grey line marks the climatological landslide frequency for each season. The grey areas indicate where the populations of the more common system are too small for the results to be significant. Note that the y -axes have different scales in each subplot.

393 those moist southwesterlies into the central or eastern
 394 Himalaya instead. We will explore this moisture flux
 395 framework more in the next section. Of additional note
 396 are the pronounced minimum in the northeastern AS –
 397 systems here would result in anomalous dry northerlies
 398 or northeasterlies passing over the Indus Basin – and
 399 the secondary maximum located towards the southern
 400 Bay of Bengal. We propose that this maximum comes
 401 about indirectly through monsoon breaks; during such
 402 periods, TD activity is highly favoured over Sri Lanka
 403 and the southern Bay of Bengal (Deoras et al., 2020),
 404 meanwhile the monsoon westerly jet is deflected north,
 405 where it impinges upon the western Himalaya. Mon-
 406 soonal TDs are climatologically far less frequent in this
 407 region than over the head of the Bay of Bengal or within
 408 the monsoon trough, so this rainfall signal may not be
 409 immediately obvious. We will explore this more in the
 410 next section.

411 Along with system location, system intensity may
 412 also be an important control on landslide frequency.
 413 For example, a strong low-pressure system over central
 414 India would be capable of providing much larger mois-

ture flux to the Indus Basin than a very weak one. To
 415 determine this relationship, we consider only systems
 416 within 2000 km of the landslide, which excludes the up-
 417 stream WDs and monsoon break TDs discussed previ-
 418 ously. The probability of a landslide occurrence is then
 419 computed at each percentile of system intensity (using
 420 850 hPa relative vorticity for TDs and 350 hPa relative
 421 vorticity for WDs), such that the zeroth percentile in-
 422 cludes all systems, the fiftieth percentile includes those
 423 stronger than the median, and so on. These intensity–
 424 probability charts are shown in Fig. 5. For October–
 425 April (left panel), we see that WD intensity has very
 426 little bearing on UIB landslide probability. A maxi-
 427 mum at about the sixtieth percentile corresponds to a
 428 frequency of 5.5% day $^{-1}$, only marginally higher than
 429 the climatological value of 5% day $^{-1}$. The presence of
 430 strong TDs during the winter is, on average, detri-
 431 mental to landslide probability, which falls below 4% day $^{-1}$
 432 at the fiftieth percentile of TD intensity. This is corrob-
 433 orated by Fig. 4(a), since TDs are much more common
 434 in the Arabian Sea during winter than summer. During
 435 May–September (right panel), we see that TD intensity
 436

437 is strongly correlated with landslide occurrence, which
438 is 50% higher during the passage of the most intense
439 TDs (i.e. eightieth percentile and up) than for the aver-
440 age. The same is true of WDs, but they are rare during
441 the summer months.

442 In summary, there is a significantly increased chance
443 of a landslide in the UIB during winter if a WD is po-
444 sitioned at or around 30°N either over or \sim 2000 km to
445 the west of the Indus Basin. The intensity of the WD is
446 not important. There is a significantly increased chance
447 of a landslide in the UIB during the summer monsoon if
448 a TD is present along the southern boundary of the cli-
449 matological location of the monsoon trough, and within
450 2000 km of the basin. Stronger TDs result in a further
451 increase in landslide probability.

452 3.2 Synoptic controls on precursor pre- 453 cipitation

454 We now know that system location (and in some cases
455 intensity) as well as precipitation is important in fore-
456 casting landslide occurrence. Here, we will now explore
457 the relationship between the two. We start by com-
458 paring mean precipitation on days in which a landslide
459 occurs in the UIB for instances where a TD or WD is
460 within 2000 km with instances where they are not, as
461 shown in Fig. 6. This is a relatively strict criterion,
462 as we will see, but still gives a respectable sample size:
463 32 out of 116 winter UIB landslides occur with a WD
464 within 2000 km and 47 out of 211 summer UIB land-
465 slides occur with a TD within 2000 km. During winter
466 UIB landslides (Fig. 6(a)), the presence of a local WD
467 causes heavier precipitation over the basin as a whole,
468 but also results in the region of heaviest precipitation
469 moving northeastwards, penetrating deeper into the Hi-
470 malayan range (see right panel). We might expect this
471 to result in landslides also occurring deeper into the
472 Himalaya (i.e. further to the northeast) when a WD

473 is present, but the difference in mean landslide loca-
474 tion between the two populations (WD present and no
475 WD present) is not statistically significant. What are
476 the reasons for these differences in precipitation? As
477 discussed earlier, WDs are the major source of winter
478 precipitation in the UIB, but there is also a consider-
479 able contribution from smaller-scale cloudbursts and lo-
480 calised orographic precipitation. These smaller storms
481 do not usually result in significant moisture flux into
482 the UIB, unlike WDs, and thus provide more isolated
483 rainfall and snowfall, which is what we see in the right
484 panel of Fig. 6(a). Cloudbursts have been previously
485 been associated with cases of severe landslides in the
486 western Himalaya (Mishra, 2015). The broad mois-
487 ture flux commonly associated with WDs can penetrate
488 further inland than the weaker, smaller-scale flux as-
489 sociated with cloudbursts and orographic storms, and
490 so this may also be the reason for the enhanced up-
491 slope precipitation. WDs also bring some additional
492 moisture along the subtropical westerly jet (e.g. Singh
493 et al., 1981), which impacts orography at higher lati-
494 tudes than southwesterly moisture flux from the AS.

495 During monsoonal UIB landslides (Fig. 6(b)), the
496 presence of a nearby TD causes a significant intensifi-
497 cation of the rainfall band along the western Himalaya
498 compared to when one is not present. As discussed ear-
499 lier, this is likely due to an intensification of the mon-
500soon trough combined with an anomalously southern
501 TD, resulting in anomalously large southeasterly mois-
502 ture flux penetrating deep into the Indus Basin. The
503 region of north India to the east of the Indus Basin,
504 south of the central Himalaya, experiences simultane-
505 ous anomalous drying. It is unlikely that this is due
506 to monsoon breaks, the secondary cause proposed ear-
507 lier, as we have filtered out contributions from the more
508 distant TDs that would be associated with this – this
509 is in fact confirmed by extending the map southwards

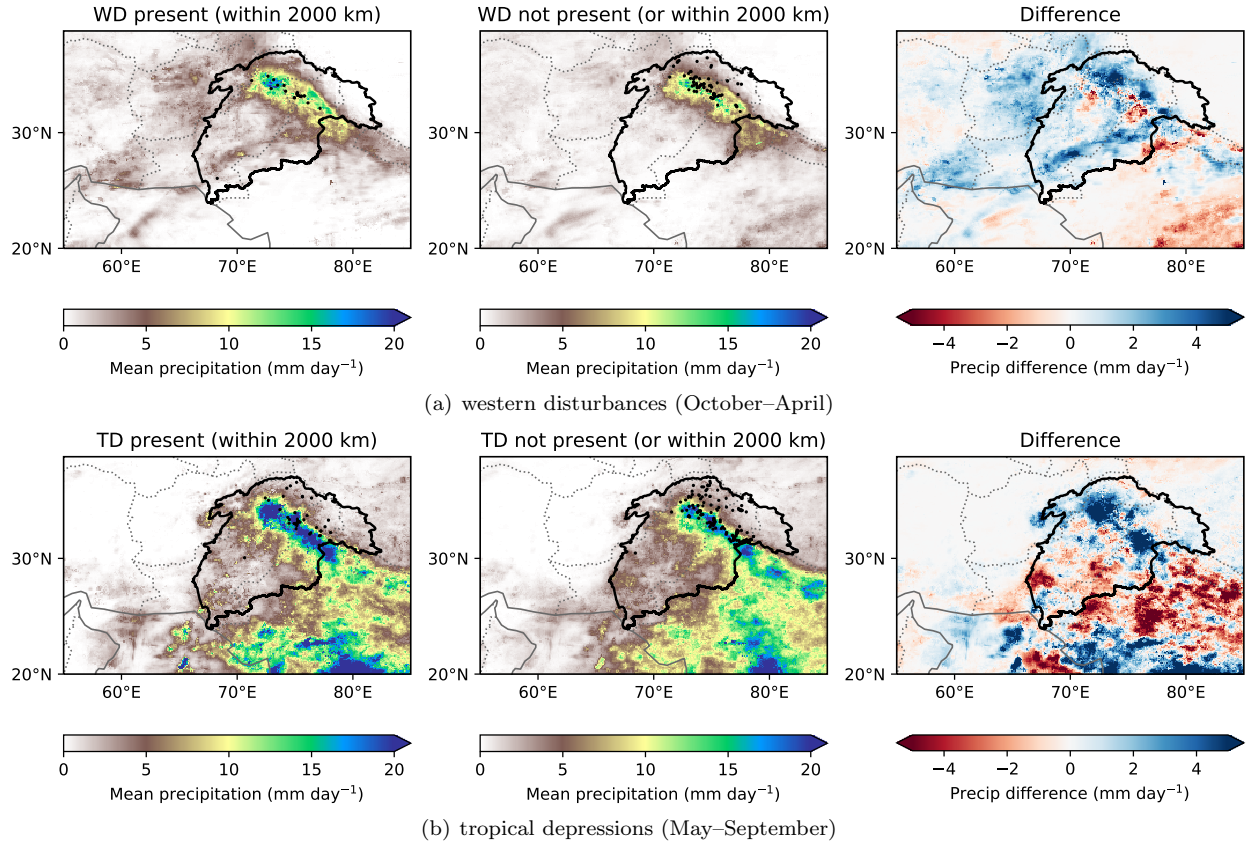


Figure 6: Mean precipitation [mm day^{-1}] on days in which a landslide occurred in the UIB in (a) October to April and (b) May to September. Separated into days where (a) a WD or (b) a TD (b) is within 2000 km of the landslide (left panels) and days where the respective system is either absent or farther than 2000 km away (middle panels). The right panels show the difference between the two. Individual landslide locations are marked with black dots. Precipitation data from GPM-IMERG.

The same figure, computed using IMDAA reanalysis, is shown in supplementary Fig. S2.

(not shown), which shows excess rainfall over much of the monsoon core zone. Instead, we propose that TDs over central India, which as we previously showed, were likely to be further south than their climatology, no longer cause moist barrier flow southeasterlies along the central Himalayan foothills; rather, they advect moisture towards the UIB from further south.

We will now test and explore these claims, and those made regarding WDs, in a moisture flux framework. Fig. 7 is constructed in the same way as Fig. 2, but instead uses vertically integrated moisture flux. The composites in Fig. 7(a) confirm our earlier hypothesis that the presence of a local WD during or immediately before a UIB landslide results in a much wider and stronger branch of westerly/southwesterly moisture flux over the Indus Basin than during its absence.

This causes more widespread precipitation and deeper penetration of moisture into the continent, and hence greater precipitation deeper into the mountain ranges, as we saw in Fig. 2(a). The scale and westward (i.e. upstream) extent of this anomalous moisture flux suggests that upstream WDs may also play an important role, though further work is needed to confirm this. We also see that during landslide days when a WD is not present (or within 2000 km), there is still a significant easterly atmospheric river passing over the Indus Basin. Though it is located too far south to provide significant moisture to the foothills or mountains where landslides are most frequent, it does show evidence of northward excursions that would provide a sufficient source of moisture for cloudbursts and orographic storms, as proposed earlier.

For UIB landslides occurring during the monsoon sea-

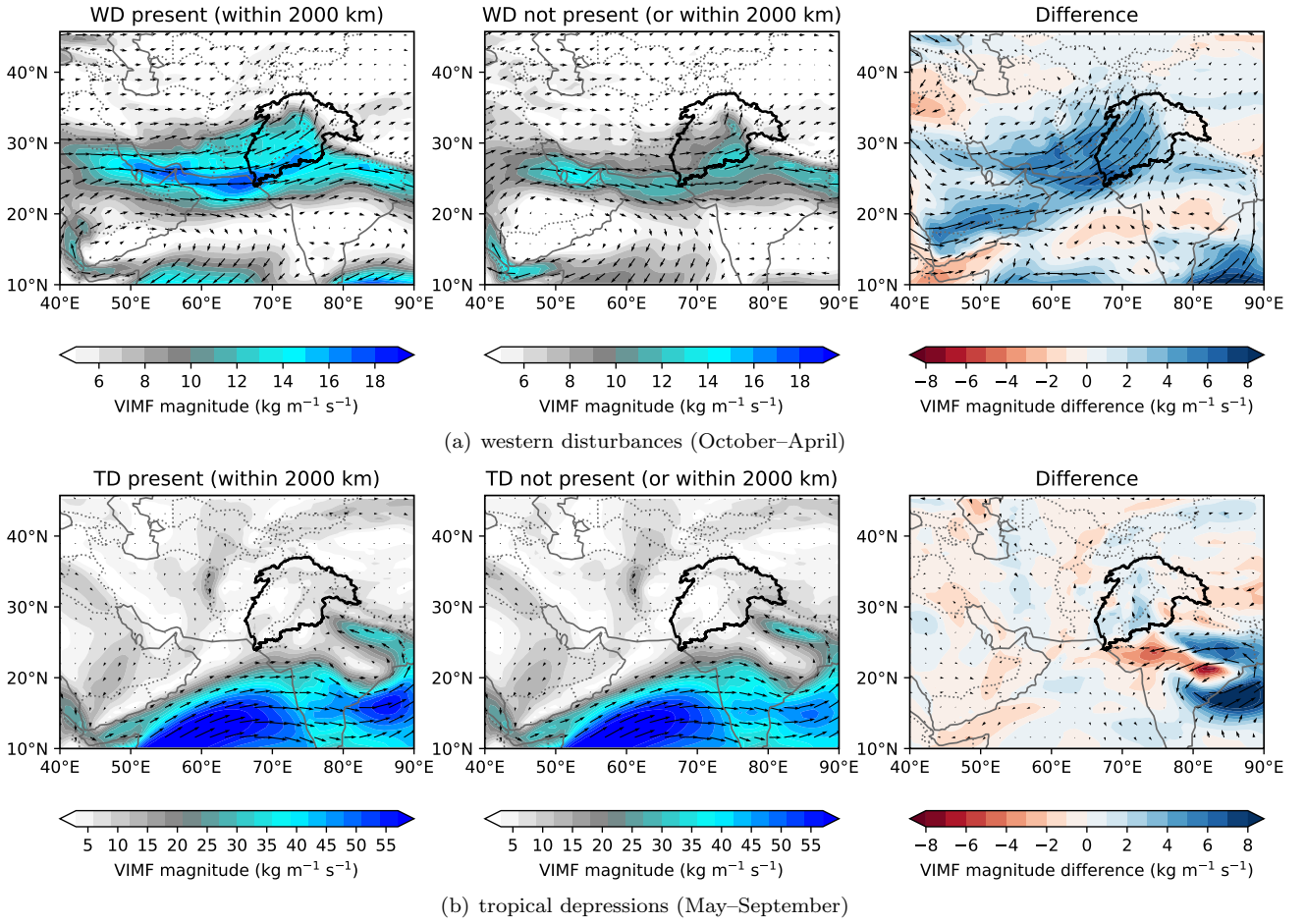


Figure 7: Mean vertically integrated moisture flux [$\text{kg m}^{-1} \text{s}^{-1}$] on days in which a landslide occurred in the UIB in (a) October to April and (b) May to September. Arrows indicate the vector field, and coloured contours show its magnitude. As in Fig. 6, these are separated into days where (a) a WD or (b) a TD (b) is within 2000 km of the landslide (left panels) and days where the respective system is either absent or farther than 2000 km away (middle panels). The right panels show the difference between the two.

son (Fig. 7(b)), the structure of the monsoon dominates, regardless of whether a TD is present or not. Strong monsoonal westerlies bring a significant quantity of moisture over the Indian peninsula, some of which reaches the BoB and is subsequently directed northward by the monsoon trough. This results in a thin but intense stream of moisture – the so-called barrier flow – reaching the edge of the Indus Basin, enough to support thunderstorms over the western Himalaya. When a TD is present, the monsoon trough is zonally extended and deepened (right panel). Perhaps most importantly, however, the whole circulation is further south than in the non-TD composite. As we hypothesised, this reduces the barrier flow (which tends to rain out over the foothills of the central Himalaya) but en-

hances southeasterly moisture flux into the Indus Basin and onto the western Himalaya and Karakoram.

We have spoken at length about precipitation occurring on the day of the landslide, which previous authors have also given the greatest importance (e.g. Dahal et al., 2008; Kirschbaum et al., 2010). However, other authors have pointed out that in addition to this, sustained antecedent rainfall, snowmelt, or runoff is required to raise the local soil moisture and reduce slope stability (Gabet et al., 2004; Kumar et al., 2014). We will now explore the relative importance of these two contributing timescales. To do this, we composite precipitation over two scales: maximum precipitation within 25 km of the landslide, and mean precipitation within 100 km of the landslide. The latter captures

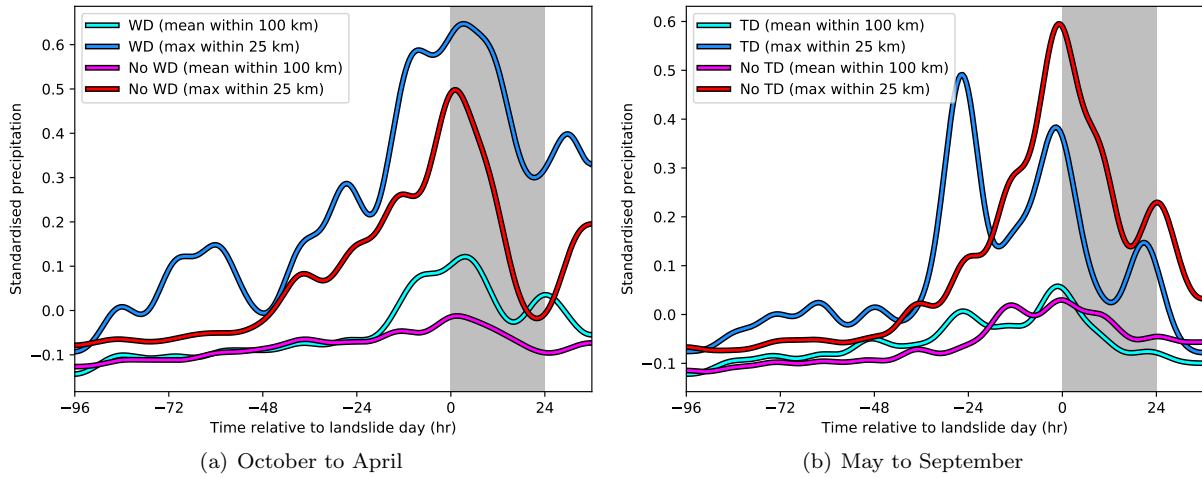


Figure 8: Antecedent rainfall, computed using GPM-IMERG, for UIB landslides occurring in (a) October–April and (b) May–September. Both mean rainfall within 100 km of the landslide (cyan, magenta) and maximum rainfall within 25 km of the landslide (blue, red) are partitioned according to whether a synoptic system was (cyan, blue) or was not (magenta, red) present and within 2000 km of the event. The grey area indicates the 24-hour period in which the landslide occurred, aligned so that 0 hr on the x-axis always corresponds to 0000 UTC. An 8-hour low-pass smoothing is applied to all data to reduce noise. The same figure, computed using IMDAA reanalysis, is shown in supplementary Fig. S3.

572 precipitation features on a larger scale (either convec-
 573 tive or stratiform), which tend to respond to both syn-
 574 optic dynamics and local forcing; the former captures
 575 high intensity small-scale precipitation, which is typi-
 576 cally convective in nature and more sensitive to local
 577 forcing. Another reason to include two scales is the
 578 spatial error in GPM-IMERG precipitation, which can
 579 suffer from anvil bias in regions of large vertical wind
 580 shear (Shrestha et al., 2015), such as south Asia under
 581 the presence of the winter subtropical westerly jet or
 582 monsoonal easterly upper-tropospheric jet. When con-
 583 structing these composites, we also align the time axes
 584 of each event such that the diurnal cycle is consistent;
 585 that is, 0 hr always represents 0000 UTC on the day
 586 in which the landslide occurs, -12 hr always represents
 587 1200 UTC on the day before the landslide occurs, and
 588 so on. This is done for two reasons: firstly, the diurnal
 589 cycle of precipitation has considerable magnitude in the
 590 orographic regions of south Asia (Ahrens et al., 2020)
 591 and so it makes sense to preserve it when compositing;
 592 secondly, precise timing of the landslide is not always
 593 available in the NASA GLC, so we can only consistently
 594 attach each landslide to the day, rather than the hour,

in which it happened.

595 Fig. 8 shows the antecedent precipitation timeline for
 596 all UIB landslides in the catalogue, partitioned by sea-
 597 son, scale, and whether a WD/TD was present and
 598 within 2000 km. During winter landslides, the 100 km
 599 mean precipitation differs little from its climatology in
 600 the absence of a WD. When a WD is present, how-
 601 ever, there is a significant increase in antecedent rain-
 602 fall, starting at about 0600 UTC on the day before the
 603 landslide (i.e. -18 hours). This lends further support to
 604 our claim that non-WD winter landslides are caused by
 605 very localised events such as cloudbursts, which would
 606 have little impact on precipitation over scales of 100 km
 607 or so. On the smaller 25-km scale, the WD cases again
 608 have higher precipitation rates than non-WD cases, and
 609 spread over a longer period, too: a positive anomaly in
 610 precipitation extends back three days prior to the land-
 611 slide when a WD is present, but only two days when it
 612 is not. In summary, winter landslides associated with
 613 WDs receive more precipitation for longer and on a
 614 larger scale; therefore, they are likely to be more se-
 615 vere, given the positive correlation between antecedent
 616 rain rate and landslide fatalities (Froude and Petley,
 617

618 2018).

619 During summer landslides (Fig. 8(b)), the effect of a
620 local TD is less clear than it was for WDs in the winter.
621 This is because, as we saw in Fig. 7(b), the presence of
622 a TD does not modulate the synoptic-scale dynamics
623 or synoptic-scale moisture flux over the Indus Basin in
624 the way that a WD does. Even so, there are some in-
625 teresting features in the antecedent rainfall timelines.
626 The mean rainfall within 100 km is never significantly
627 higher than the climatology, regardless of whether a
628 TD is present or not, highlighting the role of small-
629 scale convective storms in producing the rainfall. The
630 maximum rainfall within 25 km shows a very prominent
631 diurnal cycle in both TD and non-TD cases, peaking at
632 0000 UTC (0530 LT), in agreement with satellite obser-
633 vations of the region (Sahany et al., 2010). When a TD
634 is present, the highest rate occurs at 0000 UTC on the
635 preceding day, with a second, smaller peak occurring at
636 0000 UTC on the day of the landslide itself. For cases
637 without a local TD, there is a singular peak, larger than
638 for TDs, at 0000 UTC on the day of the landslide. It
639 is not clear what the source of this difference is, but we
640 hypothesise that a likely cause is that monsoonal TDs
641 provide a steadier (i.e. longer-lived) source of moisture
642 to the UIB than surges in barrier flow. High rainfall
643 the day before the landslide means that less rainfall
644 is then needed to trigger it on the following day. In
645 summary, the majority of summer monsoon landslides
646 in the UIB occur as the result of small-scale storms,
647 whether or not a TD is present. If a TD is present,
648 however, antecedent rainfall is considerably higher the
649 day before the landslide, resulting in favourable con-
650 ditions for one to be triggered by lighter rainfall the next
651 day. Comparison of the results from IMDAA, shown in
652 Fig. S3, with Fig. 8 confirms our findings. However, the
653 reader will have noticed that the diurnal cycle of IM-
654 DAA rainfall has a much larger amplitude. Errors in

655 this amplitude are common in models and reanalyses,
656 such as IMDAA, that use convective parameterisation
657 (e.g. Dirmeyer et al., 2012).

658 3.3 Discussion

659 One of the key research questions we asked in the in-
660 troduction was whether we can improve landslide pre-
661 dictability through an improved understanding of the
662 meteorology that causes episodes of heavy precipita-
663 tion in the UIB. We have shown that UIB landslide fre-
664 quency is highly sensitive to specific attributes of both
665 nearby WDs and nearby TDs, such as intensity (in the
666 case of TDs), location, and associated large-scale mois-
667 ture flux patterns. Combined, these results could be of
668 value to local forecasters looking to assess landslide risk
669 in the UIB in short-range forecasts. This may be fur-
670 ther improved when used in conjunction with the south
671 Asian weather regime analysis presented in Neal et al.
672 (2020).

673 One shortcoming of this work is the uncertainty in-
674 troduced by the significant relationship between under-
675 lying geology (e.g., lithology, geomorphology and land
676 use) and the relative importance of antecedent rainfall.

677 We are also able to make some hypotheses about how
678 climate change will affect UIB landslides in the future,
679 notwithstanding additional effects from deforestation or
680 construction. Monsoonal TDs are projected to move
681 poleward and decline in frequency Sandeep et al. (2018).
682 Given that UIB landslides favour TDs further south
683 than usual, both changes would contribute to a decline
684 in summer UIB landslide risk. However, a warmer at-
685 mosphere can hold more moisture, and so heavy mon-
686 soonal precipitation that does occur over the UIB would
687 likely be heavier still. Thus, the individual precipitation
688 events that typically precede clusters of UIB landslides
689 would likely become rarer but more intense.

690 As discussed in the introduction, the sign of change of

691 future WD frequency remains a topic of debate. How-
692 ever, a significant poleward movement of the subtrop-
693 ical westerly jet would reduce winter UIB frequency,
694 based on our results. In contrast, previous work (Hunt
695 et al., 2020b) has shown that precipitation associated
696 with individual winter WDs is likely to get significantly
697 more intense in a warmer atmosphere and so, like above,
698 we may find that the storms that cause landslides in the
699 UIB get rarer but more intense.

700 The work presented here opens a number of impor-
701 tant questions for future research, which are briefly
702 summarised below.

- 703 • Precipitation associated with landslides is typically
704 heavier when a WD or TD is nearby. Does this re-
705 sult in landslides occurring in locations that are not
706 otherwise usually susceptible to slope instability?
- 707 • We have shown that WDs far upstream in the west-
708 erly jet can be associated with increased UIB land-
709 slide activity. They are too distant for this to be a
710 direct effect (i.e. through moisture advection), so
711 does their presence in a cluster result in amplifica-
712 tion of nearer, downstream WDs?
- 713 • Landslides occurring when neither a WD or TD
714 are present are associated with small-scale precip-
715 itation, which we have hypothesised are due to
716 mesoscale convective systems and/or cloudbursts.
717 What conditions increase the likelihood of such sys-
718 tems in the UIB? A complete inventory of convec-
719 tive system tracks in this region is required to im-
720 prove understanding of the conditions behind non-
721 WD, non-TD landslides.
- 722 • We speculated on the relationship of monsoon
723 break conditions and UIB landslides, due to the
724 secondary maximum of TD occurrence in the south
725 of the Bay of Bengal, where they are typically
726 found during monsoon breaks. Monsoon break

727 conditions often bring anomalous rainfall to north-
728 west India, but does this result in a significant in-
729 crease in landslide risk in the UIB?

730 4 Concluding remarks

731 The objective of this study was to determine and un-
732 derstand the meteorological precursors to landslides in
733 the Upper Indus Basin (UIB), a region which con-
734 tains the orography of both the western Himalaya and
735 the Karakoram. An overwhelming majority of land-
736 slides in the UIB are precipitation-triggered, rather
737 than seismic, in nature (e.g. Froude and Petley, 2018),
738 and so we used the NASA Global Landslide Catalogue
739 (GLC; Kirschbaum et al., 2010, 2015), an inventory of
740 precipitation-triggered landslides covering 2007–2015.
741 327 UIB landslides in this period were analysed in
742 combination with track databases of common tropical
743 (tropical depressions; TDs) and extratropical (western
744 disturbances; WDs) synoptic-scale systems over south
745 Asia (Hunt et al., 2018a; Hunt and Fletcher, 2019) to
746 explore the underlying statistical and meteorological
747 relationships between them. A summary of the main re-
748 sults follows.

749 4.1 Winter: October to April

750 Based on the available landslide data, and recognising
751 the biases in the GLC, UIB landslides occur on about
752 5% of all winter days, peaking in February. WDs are
753 associated, either directly or indirectly, with 61% of
754 these. UIB landslides are significantly more common
755 when a WD, and the subtropical westerly jet in which
756 they are embedded, is situated within 3–4° of 30°N.
757 WDs further north than 40°N significantly reduce the
758 likelihood of a winter UIB landslide. In contrast to po-
759 sition, WD intensity (measured using 350 hPa relative
760 vorticity) does not have a significant relationship with

761 UIB landslide likelihood. Analysis of composite precipitation
762 over the days preceding and during landslides
763 showed that winter landslides associated with WDs re-
764 ceive significantly more precipitation and over a longer
765 time period than those not associated with WDs. In ad-
766 dition, the spatial scale of precipitation preceding non-
767 WD landslides is significantly smaller (< 100 km) than
768 that of WD landslides. In both WD and non-WD land-
769 slide cases, moisture flux into the Indus Basin is pre-
770 dominantly westerly or southwesterly. In cases where a
771 WD is near, the southwesterly moisture flux is signif-
772 icantly enhanced by the associated cyclonic winds, re-
773 sulting in moisture penetrating further inland and into
774 the mountain ranges than in non-WD cases. When a
775 WD is not present, westerlies supply significantly less
776 moisture to the UIB, though occasional northward ex-
777 cursions are sufficient to support cloudbursts and thun-
778 derstorms there.

797 both cases, rainfall preceding the landslide has a strong
798 diurnal cycle peaking at local dawn and is associated
799 with relatively small-scale systems (< 100 km), such as
800 thunderstorms or mesoscale convective systems. TDs
801 are associated with higher antecedent rainfall, bringing
802 the soil closer to field capacity, and meaning that less
803 rainfall is needed to trigger the landslide on the day
804 itself. Unlike WDs, landslide likelihood is sensitive to
805 TD intensity (measured using 850 hPa relative vortic-
806 ity): TDs in the 80th percentile of intensity are about
807 50% more likely to be associated with a UIB landslide.
808

Acknowledgments

809 KMRH is funded through the Weather and Climate Sci-
810 ence for Service Partnership (WCSSP) India, a collab-
811 orative initiative between the Met Office, supported by
812 the UK Government's Newton Fund, and the Indian
813 Ministry of Earth Sciences (MoES).

779 4.2 Summer: May to September

780 UIB landslides occur on about 11% of all summer
781 (i.e. monsoon or late pre-monsoon) days, peaking in
782 August. TDs – used as a collective term for monsoon
783 low-pressure systems, monsoon depressions and other
784 synoptic-scale tropical storms – were associated with
785 60% of these. Landslides are significantly more com-
786 mon (rising to about 20% per day) when a TD is located
787 over the centre or towards the northwest of the Indian
788 peninsula, slightly to the south of the climatological
789 position of the monsoon trough. The resulting deep-
790 ening and southward adjustment of the trough causes
791 strong, moist, monsoonal southeasterlies to enter the
792 Indus Basin. For non-TD summer landslides, the re-
793 quired moisture flux is also provided by southeasterlies,
794 but these take the form of an elongated barrier flow
795 passing parallel to the Himalayan foothills, caused by
796 a northwestward extension of the monsoon trough. In

814 References

815 , ?????: Performance evaluation of latest integrated
816 multi-satellite retrievals for Global Precipitation
817 Measurement (imerg).

818 Ahmed, M. F., J. D. Rogers, and E. H. Ismail, 2014:
819 A regional level preliminary landslide susceptibility
820 study of the upper Indus river basin. *European Journal
821 of Remote Sensing*, **47** (1), 343–373.

822 Ahrens, B., T. Meier, and E. Brisson, 2020: Diur-
823 nal cycle of precipitation in the Himalayan foothills –
824 observations and model results. *Himalayan Weather
825 and Climate and their Impact on the Environment*,
826 Springer, 73–89.

827 Ashrit, R., and Coauthors, 2020: IMDAA regional re-
828 analysis: Performance evaluation during Indian sum-

829 mer monsoon season. *Journal of Geophysical Re-* 862
 830 *search: Atmospheres*, **125** (2), e2019JD030973.

831 Atta-ur Rehman, A. N., Khan, A. E. Collins, F. Qazi, 863
 832 and Coauthors, 2011: Causes and extent of environ- 864
 833 mental impacts of landslide hazard in the himalayan 865
 834 region: a case study of murree, pakistan. *Natural* 866
 835 *Hazards*, **57** (2), 413–434.

836 Baudouin, J.-P., M. Herzog, and C. A. Petrie, 2020: 867
 837 Cross-validating precipitation datasets in the Indus 868
 838 River basin. *Hydrology and Earth System Sciences*, 869
 839 **24** (1), 427–450.

840 Chevuturi, A., and A. P. Dimri, 2016: Investigation 870
 841 of Uttarakhand (India) disaster-2013 using weather 871
 842 research and forecasting model. *Natural Hazards*, 872
 843 **82** (3), 1703–1726.

844 Dahal, R. K., S. Hasegawa, A. Nonomura, M. Ya- 873
 845 manaka, S. Dhakal, and P. Paudyal, 2008: Predictive 874
 846 modelling of rainfall-induced landslide hazard in the 875
 847 lesser himalaya of nepal based on weights-of-evidence. 876
 848 *Geomorphology*, **102** (3-4), 496–510.

849 Dee, D. P., and Coauthors, 2011: The ERA-Interim 877
 850 re- 878
 851 analysis: configuration and performance of the data 879
 852 assimilation system. *Quart. J. Roy. Meteor. Soc.*, 880
 853 **137** (656), 553–597, doi:10.1002/qj.828.

854 Deoras, A., K. M. R. Hunt, and A. G. Turner, 2020: 881
 855 Large-scale influences on regional LPS activity over 882
 856 monsoonal south Asia. *Weather*, in review.

857 Dimri, A. P., 2006: Surface and upper air fields dur- 883
 858 ing extreme winter precipitation over the western him- 884
 859 alayas. *Pure Appl. Geophys.*, **163** (8), 1679–1698.

860 Dimri, A. P., and A. Chevuturi, 2016: Western 885
 861 disturbances—structure. *Western Disturbances—An Indian Meteorological Perspective*, Springer, 1–26.

862 Dimri, A. P., A. Chevuturi, D. Niyogi, R. J. Thayyen, 862
 863 K. Ray, S. N. Tripathi, A. K. Pandey, and U. C. 863
 864 Mohanty, 2017: Cloudbursts in Indian Himalayas: a 864
 865 review. *Earth-Science Reviews*, **168**, 1–23.

866 Dimri, A. P., D. Niyogi, A. P. Barros, J. Ridley, U. C. 866
 867 Mohanty, T. Yasunari, and D. R. Sikka, 2015: Western 867
 868 disturbances: a review. *Rev. Geophys.*, **53** (2), 868
 869 225–246.

870 Dirmeyer, P. A., and Coauthors, 2012: Simulating the 871
 871 diurnal cycle of rainfall in global climate models: Res- 872
 872 olution versus parameterization. *Climate Dynamics*, 872
 873 **39** (1), 399–418.

874 Froude, M. J., and D. N. Petley, 2018: Global fatal 875
 875 landslide occurrence from 2004 to 2016. *Natural Haz- 876
 876 ards and Earth System Sciences*, **18** (8), 2161–2181.

877 Gabet, E. J., D. W. Burbank, J. K. Putkonen, B. A. 877
 878 Pratt-Sitaula, and T. Ojha, 2004: Rainfall thresholds 878
 879 for landsliding in the himalayas of nepal. *Geomor- 879
 880 phology*, **63** (3-4), 131–143.

881 Ghosh, S., E. J. M. Carranza, C. J. van Westen, V. G. 881
 882 Jetten, and D. N. Bhattacharya, 2011: Selecting and 882
 883 weighting spatial predictors for empirical modeling 883
 884 of landslide susceptibility in the darjeeling himalayas 884
 885 (india). *Geomorphology*, **131** (1-2), 35–56.

886 Hewitt, K., 1998: Catastrophic landslides and their 886
 887 effects on the upper indus streams, karakoram him- 887
 888 malaya, northern pakistan. *Geomorphology*, **26** (1- 888
 889 3), 47–80.

890 Hou, A. Y., and Coauthors, 2014: The global precipita- 890
 891 tion measurement mission. *Bulletin of the American 891
 892 Meteorological Society*, **95** (5), 701–722.

893 Huffman, G. J., D. T. Bolvin, E. J. Nelkin, and 893
 894 Coauthors, 2015: Integrated Multi-satellitE Re-

895 retrievals for GPM (IMERG) technical documentation. 928
 896 *NASA/GSFC Code*, **612** (47), 2019.

897 Hunt, K. M. R., and J. K. Fletcher, 2019: The 929
 898 relationship between Indian monsoon rainfall and low- 930
 899 pressure systems. *Climate Dynamics*, **53** (3–4), 1– 931
 900 13. 932

901 Hunt, K. M. R., A. G. Turner, and R. K. H. Schiemann, 933
 902 2020a: How interactions between tropical depressions 934
 903 and western disturbances enhance heavy precipita- 935
 904 tion. *Monthly Weather Review*, in review. 936

905 Hunt, K. M. R., A. G. Turner, and L. C. Shaffrey, 937
 906 2018a: The evolution, seasonality, and impacts of 938
 907 western disturbances. *Quart. J. Roy. Meteor. Soc.*, 939
 908 **144** (710), 278–290, doi:10.1002/qj.3200.

909 Hunt, K. M. R., A. G. Turner, and L. C. Shaffrey, 940
 910 2018b: Extreme daily rainfall in Pakistan and north 941
 911 India: scale-interactions, mechanisms, and precur- 942
 912 sors. *Mon. Wea. Rev.*, **146** (4), 1005–1022. 943

913 Hunt, K. M. R., A. G. Turner, and L. C. Shaffrey, 944
 914 2019a: Falling trend of western disturbances in future 945
 915 climate simulations. *J. Climate*, **32** (16), 5037–5051. 946

916 Hunt, K. M. R., A. G. Turner, and L. C. Shaffrey, 947
 917 2019b: Representation of western disturbances in 948
 918 CMIP5 models. *J. Climate*, **32** (7), doi:10.1175/ 949
 919 JCLI-D-18-0420.1. 950

920 Hunt, K. M. R., A. G. Turner, and L. C. Shaffrey, 951
 921 2020b: The impacts of climate change on the winter 952
 922 water cycle of the western himalaya. *Climate Dynam- 953
 923 ics*, **55** (7), 2287–2307.

924 Kamae, Y., W. Mei, and S.-P. Xie, 2017: Climatolog- 954
 925 ical relationship between warm season atmospheric 955
 926 rivers and heavy rainfall over east asia. *Journal of 956
 927 the Meteorological Society of Japan. Ser. II*. 957

928 Kirschbaum, D., R. Adler, D. Adler, C. Peters-Lidard, 958
 929 and G. Huffman, 2012: Global distribution of ex- 959
 930 treme precipitation and high-impact landslides in 960
 931 2010 relative to previous years. *Journal of hydrom- 961
 932 eteorology*, **13** (5), 1536–1551. 962

933 Kirschbaum, D., S. Kapnick, T. Stanley, and S. Pascale, 934
 934 2020: Changes in extreme precipitation and land- 935
 935 slides over high mountain asia. *Geophysical Research 936
 936 Letters*, **47** (4), e2019GL085347. 937

937 Kirschbaum, D., T. Stanley, and Y. Zhou, 2015: Spatial 938
 938 and temporal analysis of a global landslide catalog. 939
Geomorphology, **249**, 4–15. 940

940 Kirschbaum, D. B., R. Adler, Y. Hong, S. Hill, and 941
 941 A. Lerner-Lam, 2010: A global landslide catalog for 942
 942 hazard applications: method, results, and limita- 943
 943 tions. *Natural Hazards*, **52** (3), 561–575. 944

944 Kirschbaum, D. B., R. Adler, Y. Hong, S. Kumar, 945
 945 C. Peters-Lidard, and A. Lerner-Lam, 2011: Ad- 946
 946 vances in landslide nowcasting: evaluation of a 947
 947 global and regional modeling approach. *Environmen- 948
 948 tal Earth Sciences*, **66** (6), 1683–1696. 949

949 Kozu, T., and Coauthors, 2001: Development of precip- 950
 950 itation radar onboard the Tropical Rainfall Measur- 951
 951 ing Mission (TRMM) satellite. *IEEE Trans. Geosci. 952
 952 Rem. Sens.*, **39**, 102–116, doi:10.1109/36.898669, 953
 URL <http://dx.doi.org/10.1109/36.898669>. 954

954 Krishnan, R., T. P. Sabin, R. K. Madhura, R. K. Vel- 955
 955 llore, M. Mujumdar, J. Sanjay, S. Nayak, and M. Ra- 956
 956 jeevan, 2018: Non-monsoonal precipitation response 957
 957 over the Western Himalayas to climate change. *Clime- 958
 958 ate Dynamics*, 1–19. 959

959 Kumar, A., R. A. Houze Jr, K. L. Rasmussen, and 960
 960 C. Peters-Lidard, 2014: Simulation of a flash flooding 961
 961 storm at the steep edge of the himalayas. *Journal of 962
 962 Hydrometeorology*, **15** (1), 212–228. 963

963 Kummerow, C., W. Barnes, T. Kozu, J. Shiue, and J. Simpson, 1998: The Tropical Rainfall
964 Measuring Mission (TRMM) sensor package.
965 *J. Atmos. Oceanic Technol.*, **15**, 809–817, doi:
966 10.1175/1520-0426(1998)015<0809:TTRMMT>2.
967 0.CO;2, URL [http://dx.doi.org/10.1175/1520-0426\(1998\)015<0809:TTRMMT>2.0.CO;2](http://dx.doi.org/10.1175/1520-0426(1998)015<0809:TTRMMT>2.0.CO;2).

970 Kummerow, C., and Coauthors, 2000: The status of
971 the Tropical Rainfall Measuring Mission (TRMM)
972 after two years in orbit. *J. Appl. Meteor.*, **39** (12),
973 1965–1982, doi:10.1175/1520-0450(2001)040<1965:
974 TSOTTR>2.0.CO;2, URL [http://dx.doi.org/10.1175/1520-0450\(2001\)040<1965:TSOTTR>2.0.CO;2](http://dx.doi.org/10.1175/1520-0450(2001)040<1965:TSOTTR>2.0.CO;2).

976 Mamadjanova, G., S. Wild, M. A. Walz, and G. C.
977 Leckebusch, 2018: The role of synoptic processes in
978 mudflow formation in the piedmont areas of uzbek-
979 istan. *Natural Hazards and Earth System Sciences*,
980 **18** (11), 2893–2919.

981 Mishra, A., 2015: Cloudburst and landslides in uttarak-
982 hand: A nature’s fury. *Mausam*, **66** (1), 139–144.

983 Neal, R., J. Robbins, R. Dankers, A. Mitra, A. Jayaku-
984 mar, E. Rajagopal, and G. Adamson, 2020: Deriving
985 optimal weather pattern definitions for the represen-
986 tation of precipitation variability over India. *Interna-
987 tional Journal of Climatology*, **40** (1), 342–360.

988 Petley, D., 2012: Global patterns of loss of life from
989 landslides. *Geology*, **40** (10), 927–930.

990 Petley, D. N., G. J. Hearn, A. Hart, N. J. Rosser,
991 S. A. Dunning, K. Oven, and W. A. Mitchell, 2007:
992 Trends in landslide occurrence in nepal. *Natural haz-
993 ards*, **43** (1), 23–44.

994 Prakash, S., A. K. Mitra, A. AghaKouchak, Z. Liu,
995 H. Norouzi, and D. S. Pai, 2018: A preliminary as-
996 sessment of GPM-based multi-satellite precipitation
estimates over a monsoon dominated region. *Journal of Hydrology*, **556**, 865–876.

997 Rajeevan, M., S. Gadgil, and J. Bhate, 2010: Active
998 and break spells of the indian summer monsoon. *J. Earth. Syst. Sci.*, **119** (3), 229–247.

999 Rao, Y. P., and V. Srinivasan, 1969: Forecasting man-
1000 ual. Tech. Rep. IMD FMU Report-III 1.1, India Me-
1001 teorological Department, 40 pp.

1002 Ridley, J., A. Wiltshire, and C. Mathison, 2013:
1003 More frequent occurrence of westerly disturbances in
1004 Karakoram up to 2100. *Science of The Total Envi-
1005 ronment*, **468**, S31–S35.

1006 Sahany, S., V. Venugopal, and R. S. Nanjundiah,
1007 2010: Diurnal-scale signatures of monsoon rainfall
1008 over the Indian region from TRMM satellite observa-
1009 tions. *Journal of Geophysical Research: Atmospheres*,
1010 **115** (D2).

1011 Saleem, J., S. S. Ahmad, A. Butt, and Coauthors,
1012 2020: Hazard risk assessment of landslide-prone sub-
1013 himalayan region by employing geospatial modeling
1014 approach. *Natural Hazards: Journal of the Interna-
1015 tional Society for the Prevention and Mitigation of
1016 Natural Hazards*, 1–18.

1017 Sandeep, S., R. S. Ajayamohan, W. R. Boos, T. P.
1018 Sabin, and V. Praveen, 2018: Decline and poleward
1019 shift in Indian summer monsoon synoptic activity in
1020 a warming climate. *Proc. Natl. Acad. Sci. (USA)*,
1021 **115** (11), 2681–2686.

1022 Sengupta, A., S. Gupta, and K. Anbarasu, 2010: Rain-
1023 fall thresholds for the initiation of landslide at lanta
1024 khola in north sikkim, india. *Natural hazards*, **52** (1),
1025 31–42.

1026 Shrestha, D., R. Deshar, and K. Nakamura, 2015:
1027 Characteristics of summer precipitation around the
1028

1031 Western Ghats and the Myanmar West Coast. *Inter-*
1032 *national journal of atmospheric sciences*, **2015**.

1033 Singh, M. S., A. V. R. K. Rao, and S. C. Gupta, 1981:
1034 Development and movement of a mid tropospheric
1035 cyclone in the westerlies over india. *Mausam*, **32** (1),
1036 45–50.

1037 You, Q.-L., G.-Y. Ren, Y.-Q. Zhang, Y.-Y. Ren, X.-
1038 B. Sun, Y.-J. Zhan, A. B. Shrestha, and R. Krish-
1039 nan, 2017: An overview of studies of observed cli-
1040 mate change in the Hindu Kush Himalayan (HKH)
1041 region. *Advances in Climate Change Research*, **8** (3),
1042 141–147.

1043 Zhang, J., and Coauthors, 2019: How size and trigger
1044 matter: analyzing rainfall-and earthquake-triggered
1045 landslide inventories and their causal relation in the
1046 koshi river basin, central himalaya. *Natural Hazards*
1047 & Earth System Sciences